Earth and Planetary Science Letters 537 (2020) 116163

Contents lists available at ScienceDirect

Earth and Planetary Science Letters

www.elsevier.com/locate/epsl

Deep and rapid thermo-mechanical erosion by a small-volume lava flow

Gallant E.[a,b,*], Deng F.[a], Connor C.B.[a], Dixon T.H.[a], Xie S.[a], Saballos J.A.[c], Gutiérrez C.[c], Myhre D.[d], Connor L.[a], Zayac J.[e], LaFemina P.[f], Charbonnier S.[a], Richardson J.[g,h], Malservisi R.[a], Thompson G.[a]

[a] University of South Florida, School of Geosciences, United States of America
[b] University of Cambridge, Department of Geography, United Kingdom
[c] Instituto Nicaragüense de Estudios Territoriales, Nicaragua
[d] University of South Florida, College of Marine Science, United States of America
[e] Earth and Environmental Sciences Program, The Graduate Center, City University of New York, United States of America
[f] Pennsylvania State University, Department of Geosciences, United States of America
[g] NASA Goddard Space Flight Center, United States of America
[h] University of Maryland, Department of Astronomy, United States of America

ARTICLE INFO

Article history:
Received 2 October 2019
Received in revised form 8 February 2020
Accepted 13 February 2020
Available online xxxx
Editor: H. Handley

Keywords:
heat transfer modeling
planetary analogues
lava flow channel
volcano morphology
Momotombo

ABSTRACT

We document remarkably efficient thermo-mechanical erosion by a small-volume lava flow. Downcutting by a basaltic-andesite lava flow on the steep-sided Momotombo volcano, Nicaragua, occurred at 100 times the rate commonly reported for thermal erosion in lava flow fields, even though this flow was small-volume (0.02 km^3) and effused at a low rate for <1 week. The lava flow incised into the pyroclastic substrate up to 30 m, with erosion depth controlled primarily by thermal reduction of substrate hardness. We show that incision depth decreases, approximately exponentially, with distance along the flow path, until erosion stopped and the flow became constructional. This transition occurs 650 m from the vent on a slope averaging a 32° incline. Results indicate that syn-eruptive erosion is an important morphological process on some steep-sided volcanoes that are predominantly composed of layered pyroclasts. Rapid erosion and incision increased flow run-out for the 1905 flow, which in turn directed the flow and run-out of the 2015 lava flow. Mapping and understanding these features is critical for improving lava flow hazard assessments and provides insight into the construction and growth of composite cones.

1. Introduction

Lava flows are responsible for altering landscapes on geologically short timescales. The overwhelming majority of lava flows construct topography by building raised channels and/or compound flow fields, both of which evolve through time and along-flow (Kerr et al., 2006; Dietterich and Cashman, 2014). The morphologies of flow features are mainly determined by the composition and effusion rate of the flow, as well as the pre-existing and syn-eruptive topography (Richardson and Karlstrom, 2019; Bilotta et al., 2019). These factors also control the thickness of lava flows, which in turn influence a flow's run-out distance and inundation hazard potential (Kilburn and Lopes, 1988; Dietterich et al., 2017). A small fraction of channelized flows and lava tubes erode into older surfaces during emplacement via thermal, mechanical, or thermo-mechanical processes (Greeley et al., 1998; Fagents and Greeley, 2001; Kerr, 2001; Siewert and Ferlito, 2008; Hurwitz et al., 2010, 2013).

The 1905 eruption of Momotombo volcano, Nicaragua, provides an example of thermo-mechanical erosion by a small volume (<0.02 km^3) lava flow on a steep-sided edifice (Figs. 1 and 2). We first document the morphology of the channel using a combination of satellite and terrestrial radar generated digital elevation models (DEMs) from 2012–2017. Erosion depths from the 1905 flow are then calculated by reconstructing pre-channel topography, extracting cross-sectional profiles, and calculating the maximum difference between the measured and modeled surfaces normal to the channel. We use these results to test thermal and thermo-mechanical models of erosion. Model inputs are informed by observations from Momotombo's most recent eruption in 2015, which we capture with a range of satellite and ground-based observations. We find the channel was thermo-mechanically eroded

* Corresponding author.
E-mail address: eg604@cam.ac.uk (E. Gallant).

https://doi.org/10.1016/j.epsl.2020.116163
0012-821X/

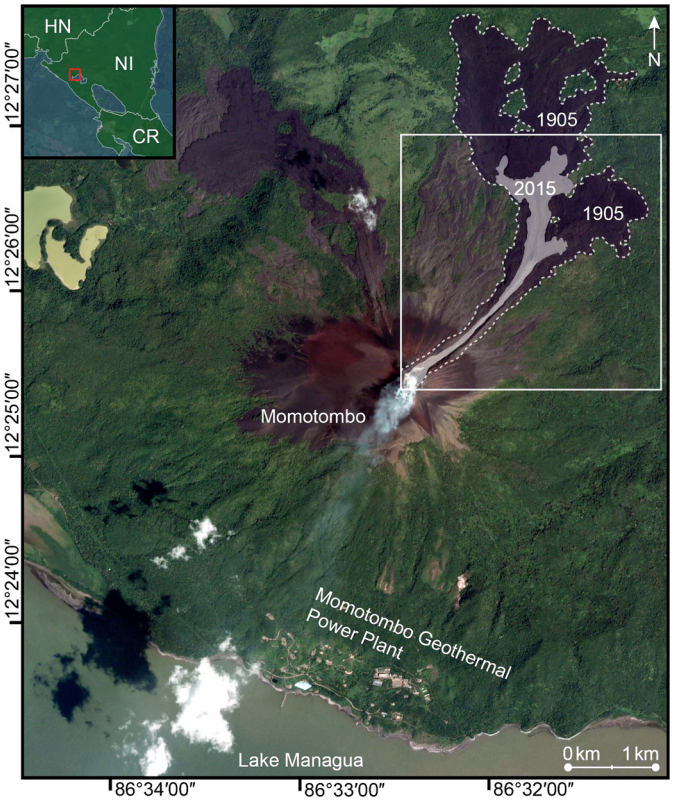

Fig. 1. Momotombo area map. The most recent volcanism (a lava flow emitted during the 2015-2016 eruption) is noted by a light-grey overlay. The 1905 eruption is noted by a dotted line. The area shown in Fig. 4 is noted by the white box. Note the widely dispersed flows that underlie the 2015 and 1905 flows. Their distribution suggests that no incised channel existed at the time of their emplacement to direct flow paths. Background image from GoogleEarth.

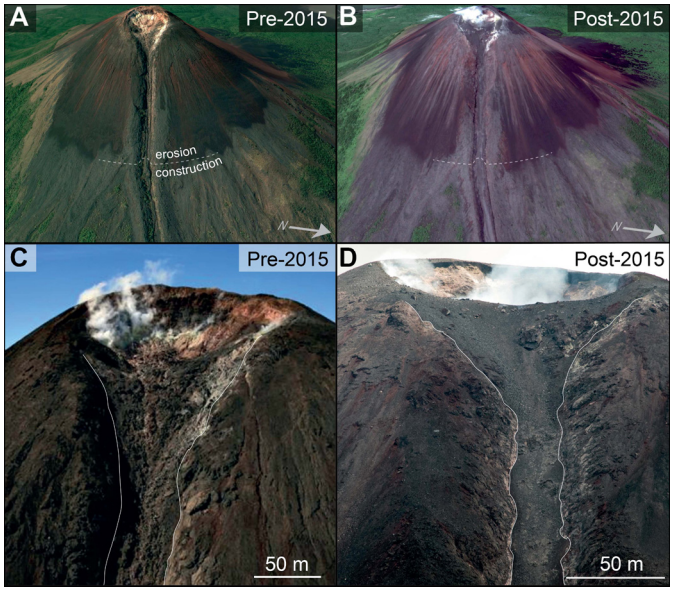

Fig. 2. Pre and post 2015-2016 eruption images of the Momotombo channel and summit. A) A pre-eruption image of the channel, where the dashed line shows the approximate transition between erosional and constructional behavior. B) Major changes in morphology can be seen in and around the summit crater, where the 2015 lava flow first filled and was then partially excavated during subsequent explosions in 2016. The pre-existing floor of the channel has been paved over by a lava flow and appears less 'rough' than the pre-eruption channel floor. Images A and B from Google Earth. C) The summit crater prior to the 2015-2016 eruption, with white lines bounding the channel. Textures within the channel indicate downslope flow. Image from INETER. D) The summit area on 6 April, 2016. Several hundred small explosions have partially excavated a small dome from December, 2015. Blocks have been deposited atop the recent lava flow and a fine, grey layer of ash from repeated pyroclastic density currents coats the channel.

by a lava flow that erupted in 1905. Additionally, we assert that thermo-mechanical erosion is an important morphological process on some steep-sided volcanoes composed predominantly of layered pyroclasts. This study is the first to look at lava flow erosion on steep sided slopes, expands our knowledge of the rate at which syn-eruptive erosion occurs, and mathematically couples thermal and mechanical models of erosion.

2. Background

2.1. Erosion by lavas

Erosion by lava has been hypothesized for the formation of rilles on both Mars (Carr, 1974; Dundas and Keszthelyi, 2014) and the Moon (Hulme, 1973; Head and Wilson, 2017; Wilson and Head, 2017), canali on Venus (Baker et al., 1992; Williams-Jones et al., 1998), and channels on Io (Schenk and Williams, 2004). Studies of active erosion by flowing lava have occurred on the island of Hawai'i during the 1972–1974 Mauna Ulu eruption and the initial stages of the 1983-2018 Pu'u O'o eruption, where erosion rates of 4 cm depth/day and 10 cm depth/day were observed in lava tubes via skylights, respectively (Peterson et al., 1994; Kauahikaua et al., 1998). Erosion by turbulent komattite flows during the Archean, responsible for large Ni-sulphide ore deposits, is also widely noted (Williams et al., 1998; Beresford et al., 2002; Staude et al., 2017).

Thermal erosion

Thermal erosion occurs when lava moves with sufficient flux and temperature to melt and incise the underlying terrain (Kerr, 2001). Thermal erosion by flowing lava requires the complete or partial melting and assimilation of a substrate into the overriding flow. A lava flow's total available thermal energy ($E_{thermal}$), sourced from advection and crystallization, is modeled as:

$$E_{thermal} = m_l[c_{pl}(T_l - T_s) + \phi F] \quad (1)$$

where m_l is the mass of the erupted lava, c_{pl} is the specific heat capacity of the lava, T_l is the erupted temperature of the lava, T_s is the inital temperature of the environment into which heat is being transferred (the substrate in this case), ϕ is the mass fraction crystallization, and F is the latent heat of fusion (Wooster et al., 1997). Lava flows are an open system where available thermal energy is eventually balanced out by heat loss through conduction, convection, and radiative heat transfer. Studies of the thermal energy balance of lava flows on Mt Etna show that upwards of 85% of energy was retained during the initial phases of the eruption, which can be used to further bound the amount of energy available to melt and erode the substrate (Wooster et al., 1997; Patrick et al., 2004). The presence of multiple heat sinks also highlights the fact that not all available thermal energy can be partitioned into eroding the substrate, so we need to quantify heat transfer between the base of the lava flow and substrate. The rate of conductive heat transfer into the substrate (i.e., the growth of a thermal boundary layer) can be modeled as:

$$\frac{dy}{dt} = \frac{\eta_T \sqrt{\kappa}}{t} \quad (2)$$

where y is the depth into the substrate, t is the duration of the flow, η_T is a dimensionless similarity variable, and κ is the thermal diffusivity (Turcotte et al., 2002; Fagents and Greeley, 2001). Thermal diffusivity is based on the relationship between thermal

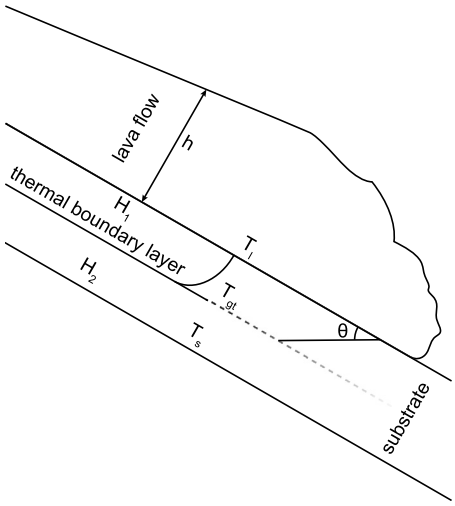

Fig. 3. Simplified model of thermal boundary formation. The energy required to melt a pyroclast-rich substrate is less than that of a lava flow because of a lower density; we can therefore substitute the peak glass transition temperature (1013 K) as the minimum temperature required to initiate melting for such substrates (Giordano et al., 2005). The formation of the thermal boundary layer shows the transition between the temperature of the lava (T_l) and the substrate (T_s). This layer defines the boundary between a thermally softened substrate (H_1) and the unaffected substrate (H_2). The height of the lava flow is noted by h and the slope of the edifice by θ.

conductivity (k), substrate density (ρ_s), and specific heat of the substrate (c_{ps}), shown as:

$$\kappa = \frac{k}{\rho_s c_{ps}} \tag{3}$$

The dimensionless similarity variable, η_T, is related to the complementary error function ($erfc$) and a dimensionless temperature ratio (θ_r),

$$\eta_T = erfc^{-1}\theta_r \tag{4}$$

The dimensionless temperature ratio, θ_r, is a measure of the relationships between the temperature at the onset of thermo-mechanical erosion of the substrate, T_e and the temperature of the lava, T_l, shown as:

$$\theta_r = \frac{T_e - T_s}{T_l - T_s} \tag{5}$$

The growth of this boundary layer, which controls the rate of thermal erosion into the substrate, is illustrated in Fig. 3 and described in Equation (2).

Mechanical erosion

Mechanical erosion occurs when the wearing material (the lava flow) is harder than the substrate (the edifice) (Sklar and Dietrich, 1998; Siewert and Ferlito, 2008; Hurwitz et al., 2010). This relationship is captured by the wear coefficient, k, determined by the relationship between the wear volume, the sliding distance of the flow, the normal load, and the hardness of the wearing material. For similar material on Mt Etna, a range of 10^{-2}-10^{-3} for k has been calculated (Siewert and Ferlito, 2008). For context, a range of $k \sim 10^{-1}$–10^{-5} characterize abrasive and erosive wear (Zum Gahr, 1998). The early stages of an eruption are most conducive to erosion because flow velocity is often highest and basal friction is also high because of the vertical load (Siewert and Ferlito, 2008; Hurwitz et al., 2010). Mechanical erosion as a function of substrate hardness can be modeled as:

$$H = \frac{k\rho g h v t \sin\theta}{d_{channel}} \tag{6}$$

where H is the hardness of the substrate, ρ is the density of the lava flow, h is the thickness of the lava flow, v is the velocity of the lava flow, θ is the slope of the edifice, and $d_{channel}$ is the depth of erosion. This equation implies that the depth of an eroded channel will be constant, so long as the velocity of the flow is constant. If the depth of the channel changes with distance, then either the velocity of the flow is changing, or the hardness, H, is changing, or both. Given that velocity changes in lava flows are readily observed and erosion appears to be a rarer phenomena, it's likely that a change in hardness is the driving factor for this process. Hardness, the ability of a material to resist deformation, is equivalent to approximately one-third of the tensile strength of the material (the yield strength). The yield strength is an exponential function of temperature, which means that H can also be modeled as a function of temperature:

$$H \approx \frac{ae^{(-bT_{i-e})}}{3} \tag{7}$$

where a and b are flow-dependent variables that vary with magma composition and e is Euler's number. This relationship describes softening of the substrate as its temperature, starting at T_i and ending at T_e, increases over time. This means that mechanical lava erosion models presented in Siewert and Ferlito (2008) can be reworked to become thermo-mechanical models. We note that experimental data have indicated that the Arrhenius relationships shown in Equation (7) break down around the glass transition point (Miller, 1963; Gottsmann and Dingwell, 2002).

2.2. Geology of Momotombo and recent activity

Momotombo (1,297 m) is located at the southern end of the Cordillera de Los Maribios in central Nicaragua (Fig. 1). The edifice is composed primarily of basaltic to basaltic andesite lavas, cinders, and other tephra that erupted during the last 4,500 years (Kirainov et al., 1988). Sixteen historical eruptions have been documented, the majority of which have been strombolian to violent strombolian (Volcanic Explosivity Index (VEI) 1-2), with several plinian events (up to VEI 4) (Global Volcanism Program, 2017). A VEI 4 eruption in 1605-1606 and large earthquake in 1610 led to the abandonment of city of León (Viejo), the capital of the region at that time (Sapper, 1925). Though the specific morphological changes to the edifice from the 1605-1606 plinian event are not well documented, it's possible that serious damage to the structural integrity of the summit occurred given the impact on surrounding municipalities (Sapper, 1925). The subsequent steady activity throughout the 1800's rebuilt the summit from cinders, agglutinate, and channelized lava flows, as shown in photographs from the late 1800's and early 1900's (Vincent, 1890; Intercontinental Railway Commission, 1898; Sapper, 1925). Ngauruhoe (New Zealand) (Hobden et al., 2002), Izalco (El Salvador) (Carr and Pontier, 1981), and Cerro Negro (Nicaragua) (Hill et al., 1998; Courtland et al., 2012) have built moderately sized pyroclastic cones in only a few hundred years and can provide further insight into rapid rates of edifice construction.

The 1905 eruption (VEI 2) occurred between January 16–21 (Sapper, 1925). The basaltic andesite lava flow was accompanied by an eruptive column of sufficient height to deposit ash 15 km to the west on the city of León. The effusive component consisted of an eruptive volume of $<0.02\,km^3$ of basaltic andesite (Fig. 1). Intermittent explosions occurred that sent incandescent blocks and bombs "a great distance" from the crater (Sapper, 1925). First person accounts also describe destruction to the summit during the eruption, which may have resulted in the drainage of a small summit lava lake (Sapper, 1925) (Fig. 2). The 1905 eruption was followed by 110 years of quiescence, which ended on 30 November,

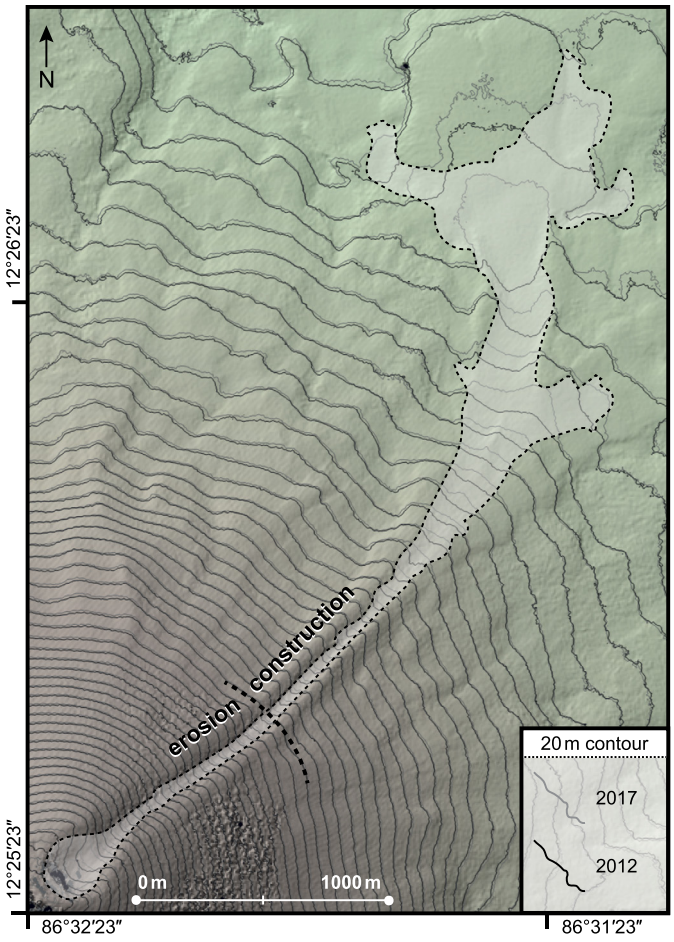

Fig. 4. Elevation contour difference measured from the 2012 and 2017 TDX DEMs. Elevation contours at 20 m intervals were mapped from the TDX datasets; the grey contours represent the 2017 elevations (post 2015-2016 eruption), and the black represent the 2012 elevations. Slight contour variations exist in areas not impacted by the 2015-2016 eruption because of the different look angles of the TDX data pairs and georeferencing uncertainties. The white infill shows the area covered by the 2015 lava flow and the thick dashed line shows the approximate area of transition between erosion and construction (~650 m).

2015. A small volume basaltic andesite lava flow was emplaced between 1 December and 7 December, 2015, and was followed by several months of intermittent explosions (Global Volcanism Program, 2017).

3. Methods and results

3.1. Digital elevation model generation

3.1.1. TanDEM-X Satellites

Digital elevation models (DEMs) were generated from TanDEM-X Satellites (TDX) and collected on 24 October, 2012 and 18 March, 2017. These DEMs, which also capture the change in topography because of the eruption in 2015–2016, allow us to obtain baseline measurements for the 1905 channel (Fig. 4) and determine if any erosion occurred during the most recent eruption. The bistatic mode of TDX allows these two satellites to fly in tandem formation and observe the same ground point simultaneously (Krieger et al., 2007). We note that the flight paths for these acquisitions were not the same, which resulted in an offset because of a heading difference of ~21°.

GAMMA software (Werner et al., 2000) was used to process the TDX SAR images to generate DEMs with the InSAR (Interferometric Synthetic Aperture Radar) technique (e.g., Deng et al., 2019). A 30-m SRTM (Shuttle Radar Topography Mission) DEM provided independent ground control points. Two (range) by two (azimuth) pixel multilooking was used to reduce speckle noise. The final DEMs have a spatial resolution of 5 × 5 meters with a vertical precision of <2 m.

3.1.2. Terrestrial radar

We employed terrestrial radar interferometry (TRI) to assess the level of noise in our topographic profiles (described below) from the 2017 TDX acquisition. Although this comparison does not give us a direct assessment of noise for the 2012 DEM (the model from which we are measuring channel incision depths), it allows direct comparison with the 2017 TDX data. TRI is a ground-based scanning radar that measures the amplitude and phase of a backscattered microwave signal. A GAMMA real aperture radar operating at Ku-band (1.74 cm wavelength) was used for this study. The TRI has one transmitting antenna and two receiving antennas, which allows for topographic mapping with a single scan (e.g. Dixon et al., 2012; Caduff et al., 2015; Voytenko et al., 2015; Xie et al., 2018; Deng et al., 2019). The resolution of the range measurements is ~1 m, and the azimuth resolution varies linearly with distance (e.g., 1.8 m at 1 km distance, 7 m at 4 km). The spatial coverage of TRI is smaller than the satellite data, but covers most of the region of interest for this study. Details of TRI data processing for DEM generation are given in Strozzi et al. (2012) and Xie et al. (2018). TRI surveys were conducted in December 2015 and April 2016. We use results from the 2016 campaign because it occurred towards the end of the eruption period and is temporally closer to the 2017 TDX acquisition. The TRI DEM has a 5 × 5 m resolution with an accuracy <5 m and covers the incised portion of the channel (Fig. S1).

3.2. Channel profiles and depth calculation

Previous GIS-based methods used to determine paleotopography of volcanic terrains (e.g., Germa et al., 2015) interpolate missing topography by connecting high points in elevation. Studies of fluvial channel erosion in steep terrain generally do not deal with incision into conical edifices (Robl et al., 2008; Fox, 2019). Additionally, these approaches model down-section and not cross-section morphology, which we require to accurately measure incision depth and extract cross-section profiles. We developed an elliptical least-square best-fit contour method to obtain incision depths along the channel on Momotombo's steep slopes to fill this application gap. We use this method to obtain channel depths and cross-channel profiles from the 2012 and 2017 TDX DEMs and the 2016 TRI DEM. Our depth measurements are minimum values, as it is likely that the eroding flow would have emplaced some volume of lava within the channel. We also use this method to determine if any incision occurred during the 2015 lava flow. Additionally, comparing the post-2015 TDX and TRI DEMs provides an indication of noise within our channel measurements.

This approach measures incision depth against modeled paleotopography created from optimized elliptical contours. A path down the channel's center was defined with a sampling density set to the resolution of the DEM (5 m for this study)(Fig. S2a). The widths of the channel and levees, determined visually, were masked out in order to separate their signal from the overall signal of the cone. A refined elliptical fit for the uppermost contour of the channel path was calculated by minimizing the mean-squared difference between the actual elevation contour and an elliptical contour. This optimized ellipse was then used to calculate a fit to the elevation contour below. This second recalculated ellipse was then fit to the next elevation contour, and so forth, until the end of the designated channel path was reached. The output of this process is a modeled paleotopography with no channel or levee structures

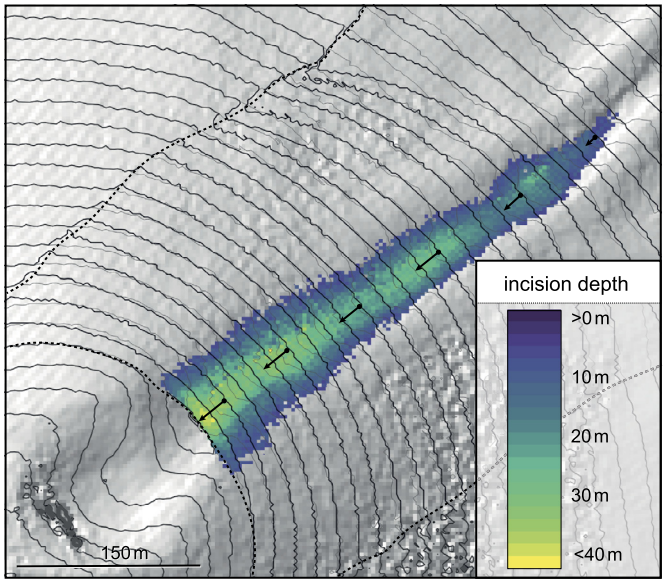

Fig. 5. Elliptical contour fit incision depth process (from 2012 DEM). The original elevation contours at 20 m intervals are noted in grey, the modeled fit in black. Incision depths, with arrows that indicate the horizontal distance between the modeled paleotopography and the current point of corresponding incision. Incision is deepest at the summit and decreases downslope until ~650 m, where the channel transitions into constructional features.

(Fig. S2b). The incision depth was calculated against the modeled paleotopography. The normal vector to the paleotopographic model was calculated at each point, spaced 5 m apart along each elliptical contour. As before, the normal vector was calculated by fitting a plane to 8 adjacent points (three from the contour above, three from the contour below, and two adjacent points from the same contour) (Fig. S2c). The DEM was then re-orientated such that the z-axis was coincident with the calculated normal vector. The incision depth was returned as a weighted average of the constituent points, with weighting criteria based on the distance of the points to the center of the plane (i.e., the point closest to the center had the greatest weight) (Fig. S2d). This process was repeated for each point along the contour, and then for every contour. This process allowed us to measure the incision depth throughout the channel while removing the conic signal of the edifice (Fig. 5). Incision depth varied from 35 m at the summit rim and tapers off to 0 at ~600 m elevation. We calculate the eroded volume of the channel to be 4×10^5 m^3. A profile of each cross-channel contour was calculated for the 2012 and 2017 TDX and 2016 TRI DEMs (Fig. 7).

Results show the pre-2015 eruption channel extended down the northeast side of the edifice from the summit and incised into the summit (Fig. 5). The 2015 lava flow follows the same path as the pre-eruption channel (Fig. 7). The elliptical contour fit method was also applied to the 2016 TRI DEM. Data gaps within the DEM were filled using a regularized spline with tension interpolation method in QGIS and the same process described above was utilized. We provide the code for this method (S1) and an additional code for a circular fit method in the Supplemental Documentation (S2).

4. Discussion

4.1. Channel origins

The difference between modeled paleotopography and the 2012 TDX DEM shows that a channel has cut into the edifice. The distribution of lava flows beneath the 1905 units, shown in Fig. 1, implies that no structure existed in this location prior to 1905 to consistently direct the path of subsequent lava flows (as was the case for the 2015 eruption). No historical reports note a leveed lava channel on the NE flank of Momotombo prior to the 1905 eruption (Vincent, 1890; Intercontinental Railway Commission, 1898; Sapper, 1925). Examination of the area surrounding Momotombo shows no down-slope deposition of sufficient volume to support a channel having carved into the NE edifice prior to the 1905 eruption by environmental erosion (e.g. hydrologic erosion) and then in-filled by subsequent lava flows. The rest of the edifice is similarly devoid of any large-scale drainage features (e.g. barrancas, rilles, or gullies). DEM analyses show the channel width is uniform from summit to low on the slopes (Fig. 4). Incised channels on other volcanoes (e.g., Merapi, Nevado del Ruiz) are generally much wider at the mouth, less consistent in width, and are less linear than Momotombo's channel because they are related to more violent hazards (e.g., pyroclastic density currents and lahars). Results also show it was unlikely that erosion occurred during the 2015 lava flow, given that it flowed over the armored channel and not a variably consolidated slope of cinders and spatter/agglutinate (Fig. 7). In the absence of evidence that suggests otherwise, we conclude that channel most likely formed during the emplacement of the 1905 lava flow.

4.1.1. Thermal erosion

The total energy emitted by the 1905 lava flow, calculated using Equation (1), is about 7×10^{16} J for an eruptive volume of 2×10^7 m^3. Taking into account the energy balance between heat sources (85% retained) and sinks (15% lost) described in Wooster et al. (1997), we calculate that 6×10^{16} J is the minimum amount of the original energy that remained within the flow. Although the length of time used to calculate this ratio for the Mount Etna eruption was greater than the duration of the Momotombo eruption, it is helpful to place a first order constraint on how much thermal energy is lost into the environment. We calculate the total energy needed to fully erode the channel is about 2×10^{14} J, by substituting the mass of the eroded section of the channel into Equation (1). Although we find that sufficient energy exists within the system to erode the substrate, we note that not all of the energy present is available for this purpose. Had all of this energy been used to erode, the thermal loss would have been sufficiently great that the emplaced flow would be much thicker and shorter than what is observed. Modeling the depth of heat transfer into the substrate as a function of time using Equation (2) estimates the growth of the substrate thermal boundary layer at 8.8 cm per day when we account for the reduced density of cinders in our thermal diffusivity calculation (~1000 kg m^{-3} for our study area). Thermal erosion rates in Hawaiian tubes and channels can reach ~10 cm per day (Kauahikaua et al., 1998); given the lower temperature of lavas erupted on Momotombo, a slower rate of thermal boundary layer growth makes sense. Given the short duration of the 1905 eruption (<1 week; Sapper, 1925), thermal erosion by itself is unlikely to have formed the observed morphology.

4.1.2. Thermo-mechanical erosion

Conceptually, once the near-subsurface reaches the threshold temperature, which we assert is the glass transition (T_e, which is about 1013 K for basaltic rocks, Giordano et al., 2005), the hotter subsurface material begins to creep/flow and is transported downhill by the lava flow. This implies that the thermal boundary layer reaches some critical thickness and is then eroded away mechanically by the lava flow. While this process surely contributes to incision of the channel, it cannot fully account for the observed depths. It is possible H varies with distance along the channel because the underlying substrate changes from very soft material at the top of the cone to harder material lower on the flanks. We reject this because the surface of the edifice is a relatively uniform slope without major lithologic changes. These results help us

understand how the material hardness of the substrate, H, is reduced over time as the lava flow moves downslope. Hardness is related to measurable mechanical properties (e.g., uniaxial compressive strength, shear/tensile strength, shear modulus). Siewert and Ferlito (2008) report H as being approximately 1/3 of the tensile strength of rock. Assuming this to be valid, and that tensile strength is approximately 1/10 of the compressive strength (e.g., Jaeger et al., 2007), then the value of H of the cinders ($\sim 4 \times 10^6$ Pa) corresponds to compressive strength in the region of $\sim$120 MPa. For comparison, basaltic lavas can have compressive strengths of over 300 MPa (e.g., Farquharson et al., 2016).

We assume that the growth and removal of the thermal boundary layer over time can be approximated as a steady state process, captured by the depth of incision at each point along the channel. An exponential was fit to the incision depth data to extract the quadradic function of $d_{channel}$ in terms of incision depth and elevation (Fig. 9). We solve for H and find that the transition from erosion to construction happens around 4×10^6 Pa. Modeling the results in this way suggests that the hardness of the substrate increases as a function of time, but note that we use depth as proxy for time. Realistically, the deepest incision points are closest to the vent because they have been exposed to erosive work for a greater amount of time. The function modeled from Equation (6) tackles that problem from the opposite perspective (i.e., it models the decrease in erosive depth, which suggests increase in hardness). We know that temperature is increasing in the substrate based on the relationships described in Equation (2), which decreases the hardness, so we revise these results and report them as a decrease in hardness over time to more accurately reflect the physical processes controlling the incision depth. Detailed historical observations list the eruption duration as six to seven days in length (Sapper, 1925). The effusive phase of the 2015 eruption persisted for the same amount of time, but emplaced the majority of the lava within the first two days. Collectively, these observations allow us to place constraints on the rate of change of hardness (Fig. 9). Future work involves laboratory determination of the tensile strength and hardness of Momotombo lavas and cinders to refine these results.

4.2. Channel growth

We calculate that the eroded volume is equal to roughly 2% of the total volume of the 1905 lava flow. Given the low eruptive temperature of basaltic andesites, it is unlikely that this material was fully assimilated into the flow. As the material heats and softens it is likely dragged downslope along the base of the flow for a short distance and then re-deposits, which creates a scalloped type signal for the measure of incision depth against elevation (Fig. 6). The thicknesses of subsequent lava flows will respond to this subtle topographic variability (i.e., more lava will be deposited in the troughs, less on the crest), which we find to be true for the 2015 flow (Fig. 6). We find no physical evidence of entrained substrate fragments at the base of the 1905 flow. Although other authors have noted geochemical evidence for assimilation of the substrate into the flow (e.g., Williams et al., 2004), geochemical similarities between recent Momotombo eruptive products make this an unlikely scenario for Momotombo. We also note a strong correlation between incision and lack of developed levees in the 2012 TDX DEM, which suggests that erosion began early on during the eruption (Fig. 7, conceptualized in Fig. S2F). This implies that levee bounded incised channels are not thermo-mechanically eroded, which is an important consideration for studies of incised channels on other planetary bodies.

Similar channels observed on the Moon exhibit nested rille structures (Hurwitz et al., 2013). These features might indicate that the tendency for extant channels to become catchments for later lava flows at Momotombo also exists for lower sloped, larger volume lava flows on the Moon. If this pattern of repeated occupation of rilles on the Moon was common then in addition to nested rilles, partially-infilled shallow rilles should exist, similar to the current channel at Momotombo, which has now been partially filled with the most recently erupted lava. While it is certainly possible that nested rilles might form from a single effusive eruption, we note that the channels on Momotombo have simple, single grooved, shapes. This could be in part due to the small volume of the flow and its short eruption timeline, or because of the high slope compared to rille-present lunar environments, which increases the efficacy of mechanical erosion (Williams-Jones et al., 1998). However, our findings that substrate hardness plays a key role in thermomechanical erosion and that this hardness significantly decreases around the glass transition indicates that thermomechanical erosion by lavas through low sloping, unconsolidated regolith might play a larger role than previously hypothesized.

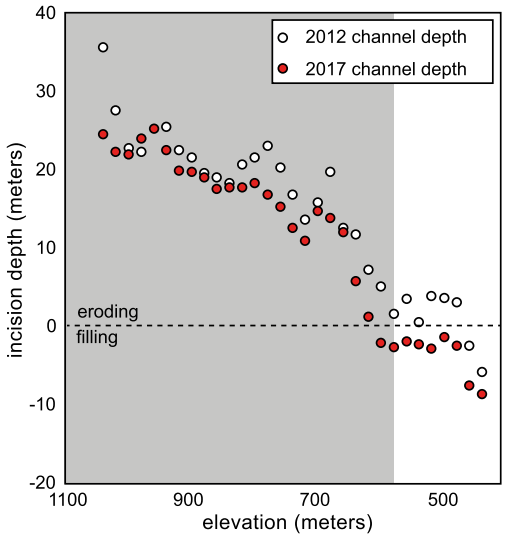

Fig. 6. Calculated channel depths at 20-m elevation intervals before and after the eruption, using the elliptical fit method described in Fig. 5. Calculated channel depths and slopes at 20-m elevation intervals before and after the eruption. White and red dots are channel depths of the pre- and post-eruption channel, respectively. The difference of the two DEMs gives us the thickness of the 2015 lava flow. The grey shading indicates the elevation range where erosion dominates (>650 m). (For interpretation of the colors in the figure(s), the reader is referred to the web version of this article.)

4.3. Morphologic implications

The depth of a thermally eroded channel is limited by the efficiency of heat transfer across the boundary between the lava flow and the substrate, the rate of heat transfer in the subsurface, and the duration of an eruption (Kerr, 2001); when combined with morphologic studies of emplacement conditions (especially time), a constraint can be placed on the maximum depth of erosion. Channels whose incision depth exceeds this threshold indicate a preferential hardness ratio of the substrate to the flow (i.e., it is softer than the overriding flow) and can therefore be used to determine the presence of pyroclastic rocks and other easily eroded terrain (e.g., unconsolidated regolith and alluvial deposits) on planetary surfaces that can only be observed remotely. Large flows on the Moon, in particular, may be worth revisiting in light of these findings (Hurwitz et al., 2013). Additionally, this suggests that the rate and depth of heat transfer for areas susceptible to incision may present a higher than normal hazard for buried infrastructure (Tsang et al., 2019).

A 1528 drawing of Momotombo, Infierno de mamea by Oviedo, shows a similar channel on the volcano's west side. A channel

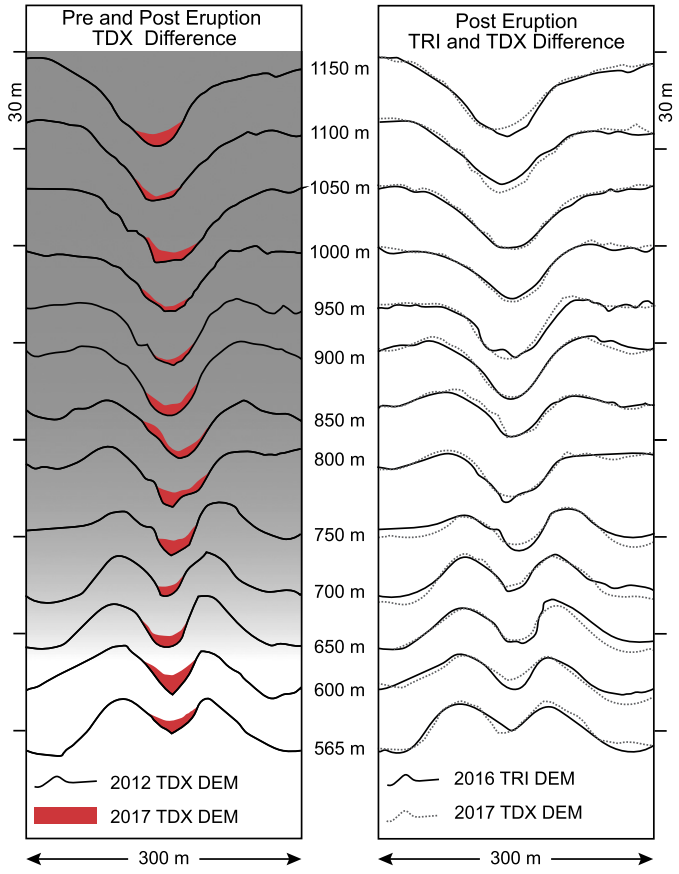

Fig. 7. Momotombo lava channel profiles. The left figure shows channel profiles from the 2012 TDX DEM and an overlay of the lava flow from 2015. The 2012 profile is noted by the solid black line, with the 2015 lava flow (imaged by the 2017 TDX acquisition) by the red polygon. The grey shading illustrates the transition of channel into a constructional feature at ~650 m. The profiles have been visually adjusted to match up topography in order to account for the 21° difference in acquisition angles. The right figure shows the difference between the 2016 TRI DEM and the 2017 TDX DEM. Comparison of the post-eruption profiles estimates the relative noise of the DEMs.

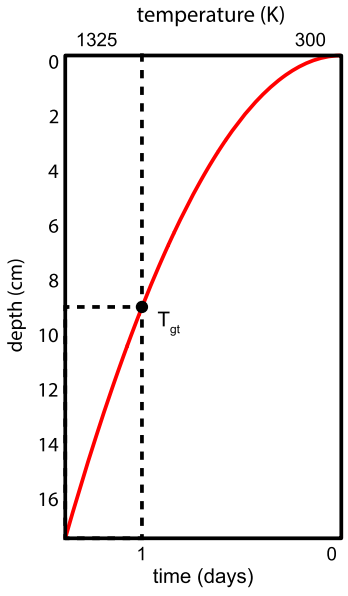

Fig. 8. Substrate thermal boundary layer. At one day, we calculate the thermal boundary layer for a flow on Momotombo to grow to 8.8 cm. Thermal erosion rates in Hawaiian tubes and channels can reach ~10 cm per day (Kauahikaua et al., 1998); given the lower temperature of lavas erupted on Momotombo, it is reasonable to assume a slower rate of thermal boundary growth.

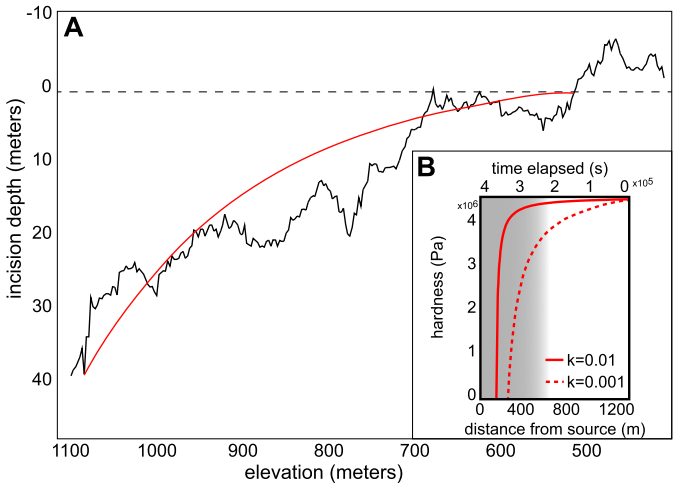

Fig. 9. Incision depth fit models. A: Depth is used as a proxy for time in order to constrain the hardness (H) of the eroded substrate. The red line indicates the exponential fit to the eroded depth as a function of elevation. The dotted line indicates the transition from erosion (below) to construction (above). B: Substrate hardness as a function of time and distance. Time elapsed is the total time the substrate is in contact with flowing lava. The grey shading illustrates the transition of channel into a constructional feature at ~650 m. We model the change of H as a function of time and distance for different values of the wear coefficient, $k = 0.01$, as the solid red line and $k = 0.001$ as the dotted red line.

on the northern flank (likely emplaced during an eruption in the second half of the 1800's (Sapper, 1925)) is also incised into the cone, and has been infilled by cinders from subsequent eruptions, which suggests the processes of slope incision and subsequent infill occurs with relative frequency on Momotombo. The preferential diversion of lava flows into incised channels for future events suggest that lava flow hazards on some steep-sided volcanoes are influenced by the creation, infill, and eventual abandonment of these structures. The channel may limit the lava flow hazard for the western flank if the next eruption is similar in size. Understanding the evolution of these features has important implications for lava flow hazards and growth patterns and erosion of composite volcanoes. Similar features can be found on Sierra Negra (Galápagos). Syn-eruptive erosion suggests a strength differential in the materials that construct some volcanic cones, which can indicate increased susceptibility to internal structural instabilities. Incision into cinder cones via flowing lava likely plays a major role in their destruction, which in turn impacts subsequent flow inundation patterns (see Table 1).

5. Conclusions

We use satellite (TDX) and terrestrial radar (TRI) DEMs to obtain a detailed record of recent changes to the edifice of Momotombo Volcano from 2012–2017, during which a VEI-2 eruption occurred. We describe a unique lava channel that incised 25–35 m into the northeast sector of the volcano near the summit and transitions into a constructional channel roughly halfway down the edifice. We assert that this feature formed erosively during the emplacement of a lava flow in 1905 and note a direct correlation between a lack of levees and incision depth. Thermal erosion alone was unable to account for the full depth of incision and we suggest that thermo-mechanical erosion is the likely cause. We examine inputs from mechanical models of erosion and determine that, based on the relationship between material hardness and shear strength, these models should be re-classified as thermo-mechanical. We propose that the transfer of heat into the substrate decreases the hardness of the material, which encourages it to flow more readily and excavate, in agreement with modeling approaches by Hup-

Table 1
Momotombo erosion model variables, input parameters, and sources.

Variable	Meaning	Value (units)	Source
N/A	volume of 1905 lava flow	2×10^7 (m^3)	this study (DEM analysis)
N/A	volume of eroded channel	4×10^5 (m^3)	this study (DEM analysis)
ρ	density of 1905 lava	2600 ($kg\,m^{-1}$)	this study
ρ_s	density of cinders	1000 ($kg\,m^{-1}$)	this study
c_l	specific heat capacity for lava	1400 ($J\,kg^{-1}$)	this study (MELTS)
T_l	lava temperature	1325 (K)	this study (FLIR)
T_s	initial substrate temperature	300 (K)	this study (FLIR)
ϕ	mass fraction crystallization	50%	this study (sample)
F	latent heat of fusion	2.5×10^5 (Jkg^{-1})	analogous flow, Siewert and Ferlito (2008)
y	depth into substrate	see Fig. 8	this study
t	eruption duration	2–5 days	Sapper (1916)
κ	thermal diffusivity	2.5×10^{-7} m^2s^{-1}	this study
η_T	similarity variable	0.3	this study
k_T	thermal conductivity	0.2 ($Wm^{-1}K^{-1}$)	Connor et al., 1997
c	specific heat capacity for cinders	800 ($J\,kg^{-1}\,K^{-1}$)	this study (MELTS)
$efrc$	complementary error function	0.4286	this study
θ_r	dimensionless similarity variable	0.7	this study
T_e	temperature for erosion initiation	1013 K	Giordano et al. (2005)
k	wear coefficient	0.01–0.001	analogous flow, Siewert and Ferlito (2008)
h	lava flow thickness (in channel)	3 m	this study (2015 flow)
v	average lava flow velocity	0.25-1.75 ($m\ s^{-1}$)	this study
θ	slope	locally variable: 5-35°	this study (DEM analysis)
$d_{channel}$	depth of erosion	0-30 (m)	this study (DEM analysis)
Model output	**Meaning**	**Value (units)**	**Source**
$E_{thermal}$	total thermal energy of 1905 flow	7×10^{16} (J)	this study
E_{eroded}	thermal energy required to erode channel	2×10^{14} (J)	this study
H	substrate hardness	see Fig. 9B	this study

pert et al. (1984) and Williams et al. (1998). We establish that the critical temperature at which this occurs is lower than previously thought, likely at the glass transition temperature (1013 K), instead of the liquidus of a given lava. We calculate the total eroded volume to be 4×10^5 m^3 and determine that erosion is likely to occur when the hardness of the substrate is less than 4×10^6 Pa. Deeply incised channels control the distribution of future flows and can also be used to infer the material properties of the substrate into which they are excavated.

Declaration of competing interest

The authors declare that they have no known competing financial interests or personal relationships that could have appeared to influence the work reported in this paper.

Acknowledgements

Funding for field work was provided by NSF EAR 1620977: Geochemical and Geophysical Observations of the 2015 Eruption of Volcan Momotombo, Nicaragua, awarded to PL, CC, and others. Deployment of the TRI was partially funded by NSF RAPID grant EAR 1546924 to THD and SC. Field support was provided by many staff members at INETER. We thank the German Aerospace Center (DLR) for providing TanDEM-X SAR data. Equipment logistics were eased by the efforts of Denis Voytenko, Milton Ordonez, and Anderson at the Servicio Geológico Colombiano. The manuscript's clarity was improved by feedback from Jen Bright and Christopher Sant. Pam Wayne and Jose Rincon were crucial in facilitating this feedback. We thank Heather Handley (editor) and reviewers Jamie Farquharson and David Williams for their quick and thoughtful feedback.

Appendix A. Supplementary material

Supplementary material related to this article can be found online at https://doi.org/10.1016/j.epsl.2020.116163.

References

Baker, V.R., Komatsu, G., Parker, T.J., Gulick, V.C., Kargel, J.S., Lewis, J.S., 1992. Channels and valleys on Venus: preliminary analysis of Magellan data. J. Geophys. Res., Planets 97 (E8), 13421.

Beresford, S., Cas, R., Lahaye, Y., Jane, M., 2002. Facies architecture of an Archean komatiite-hosted Ni-sulphide ore deposit, Victor, Kambalda, Western Australia: implications for komatiite lava emplacement. J. Volcanol. Geotherm. Res. 118 (1), 57–75.

Bilotta, G., Cappello, A., Herault, A., Del Negro, C., 2019. Influence of topographic data uncertainties and model resolution on the numerical simulation of lava flows. Environ. Model. Softw. 112, 1–15.

Caduff, R., Schlunegger, F., Kos, A., Wiesmann, A., 2015. A review of terrestrial radar interferometry for measuring surface change in the geosciences. Earth Surf. Process. Landf. (2), 208.

Carr, M., 1974. The role of lava erosion in the formation of lunar rilles and martian channels. Icarus 22 (1), 1–23.

Carr, M.J., Pontier, N.K., 1981. Evolution of a young parasitic cone towards a mature central vent. Izalco and Santa Ana volcanoes in El Salvador, Central America. J. Volcanol. Geotherm. Res. 11, 277–292.

Connor, C., Lichtner, P., Conway, F., Hill, B., Ovsyannikov, A., Federchenko, I., Doubik, Y., Shapar, V., Taran, Y.A., 1997. Cooling of an igneous dike 20 yr after intrusion. Geology (8), 711.

Courtland, L.M., Kruse, S.E., Connor, C.B., Connor, L.J., Savov, I.P., Martin, K.T., 2012. GPR investigation of tephra fallout, Cerro Negro volcano, Nicaragua: a method for constraining parameters used in tephra sedimentation models. Bull. Volcanol. (6), 1409.

Deng, F., Rodgers, M., Xie, S., Dixon, T., Charbonnier, S., Gallant, E., Lopez-Velez, C., Ordonez, M., Malservisi, R., Voss, N., Richardson, J., 2019. High-resolution dem generation from spaceborne and terrestrial remote sensing data for improved volcano hazard assessment — a case study at Nevado del Ruiz, Colombia. Remote Sens. Environ. 233, 1113–1148.

Dietterich, H., Lev, E., Chen, J., Richardson, J., Cashman, K., 2017. Benchmarking computational fluid dynamics models of lava flow simulation for hazard assessment, forecasting, and risk management. J. Appl. Volcanol. 6 (1), 1.

Dietterich, H.R., Cashman, K.V., 2014. Channel networks within lava flows: formation, evolution, and implications for flow behavior. J. Geophys. Res., Earth Surf. 119 (8), 1704.

Dixon, T.H., Voytenko, D., Lembke, C., Peña, S., Howat, I., Gourmelen, N., Werner, C., Oddsson, B., 2012. Emerging technology monitors ice-sea interface at outlet glaciers. Eos 93 (48), 497.

Dundas, C.M., Keszthelyi, L.P., 2014. Emplacement and erosive effects of lava in south Kasei Valles, Mars. J. Volcanol. Geotherm. Res. 282, 92–102.

Fagents, S.A., Greeley, R., 2001. Factors influencing lava-substrate heat transfer and implications for thermomechanical erosion. Bull. Volcanol. (8), 519.

Farquharson, J.I., Heap, M.J., Baud, P., 2016. Strain-induced permeability increase in volcanic rock. Geophys. Res. Lett. 11, 603.
Fox, M., 2019. A linear inverse method to reconstruct paleo-topography. Geomorphology 337, 151–164.
Germa, A., Lahitte, P., Quidelleur, X., 2015. Construction and destruction of Mont Pelée volcano: volumes and rates constrained from a geomorphological model of evolution. J. Geophys. Res., Earth Surf. 120 (7), 1206.
Giordano, D., Nichols, A.R., Dingwell, D.B., 2005. Glass transition temperatures of natural hydrous melts: a relationship with shear viscosity and implications for the welding process. J. Volcanol. Geotherm. Res. (1–2), 105.
Global Volcanism Program, 2017. Report on Momotombo (Nicaragua). In: Venzke, E. (Ed.), Bulletin of the Global Volcanism Network, vol. 42:1. Smithsonian Institution.
Gottsmann, J., Dingwell, D.B., 2002. The thermal history of a spatter-fed lava flow: the 8-ka pantellerite flow of Mayor Island, New Zealand. Bull. Volcanol. 64 (6), 410–422.
Greeley, R., Fagents, S.A., Scott Harris, R., Kadel, S.D., Williams, D.A., Guest, J.E., 1998. Erosion by flowing lava: field evidence. J. Geophys. Res. (B11), 27.
Head, J.W., Wilson, L., 2017. Generation, ascent and eruption of magma on the Moon: new insights into source depths, magma supply, intrusions and effusive/explosive eruptions (Part 2: Predicted emplacement processes and observations). Icarus 283 (Lunar Reconnaissance Orbiter - Part II), 176–223.
Hill, B.E., Connor, C.B., Jarzemba, M.S., La Femina, P.C., Navarro, M., Strauch, W., 1998. 1995 eruptions of Cerro Negro volcano, Nicaragua, and risk assessment for future eruptions. Geol. Soc. Am. Bull. (10), 1231.
Hobden, B.J., Houghton, B.F., Nairn, I.A., 2002. Growth of a young, frequently active composite cone: Ngauruhoe volcano, New Zealand. Bull. Volcanol. (6), 392.
Hulme, G., 1973. Turbulent lava flow and the formation of lunar sinuous rilles. Mod. Geol. 4, 107–117.
Huppert, H., Sparks, R., Turner, J., 1984. Emplacement and cooling of komatiite lavas. Nature 309, 19–22.
Hurwitz, D.M., Fassett, C.I., Head, J.W., Wilson, L., 2010. Formation of an eroded lava channel within an Elysium Planitia impact crater: distinguishing between a mechanical and thermal origin. Icarus 210 (2), 626–634.
Hurwitz, D.M., Head, J.W., Hiesinger, H., 2013. Lunar sinuous rilles: distribution, characteristics, and implications for their origin. Planet. Space Sci. 79 (80), 1–38.
Intercontinental Railway Commission, 1898. A Condensed Report of the Transactions of the Commission and of the Surverys and Explorations of its Engineers in Central and South America.
Jaeger, J.C., Cook, N.G.W., Zimmerman, R.W., 2007. Fundamentals of Rock Mechanics. Electronic resource. Blackwell Pub.
Kauahikaua, J., Cashman, K.V., Mattox, T.N., Heliker, C.C., Hon, K.A., Mangan, M.T., Thornber, C.R., 1998. Observations on basaltic lava streams in tubes from Kīlauea Volcano, Island of Hawai'i. J. Geophys. Res., Solid Earth 103 (B11), 27303.
Kerr, R.C., 2001. Thermal erosion by laminar lava flows. J. Geophys. Res. (11), 26.
Kerr, R.C., Griffiths, R.W., Cashman, K.V., 2006. Formation of channelized lava flows on an unconfined slope. J. Geophys. Res., Solid Earth (1978–2012) 111 (B10).
Kilburn, C.R.J., Lopes, R.M.C., 1988. The growth of AA lava flow fields on Mount Etna, Sicily. J. Geophys. Res., Solid Earth 93 (B12), 14759–14772.
Kirainov, V., Melekestev, I., Ovsyannikov, A., Andreev, V., 1988. Reconstruction of the eruptive activity of Momotombo volcano (Nicaragua) to assess volcanic hazards. 495–498.
Krieger, G., Moreira, A., Fiedler, H., Hajnsek, I., Werner, M., Younis, M., Zink, M., 2007. TanDEM-X: a satellite formation for high-resolution SAR interferometry. IEEE Trans. Geosci. Remote Sens. (11), 3317.
Miller, A.A., 1963. Free volume and viscosity of liquids: effects of temperature. J. Phys. Chem. 67 (5), 1031–1035.
Patrick, M.R., Dehn, J., Dean, K., 2004. Numerical modeling of lava flow cooling applied to the 1997 Okmok eruption: approach and analysis. J. Geophys. Res. (3), B03202. https://doi.org/10.1029/2003jb002537.
Peterson, D.W., Holcomb, R.T., Tilling, R.I., Christiansen, R.L., 1994. Development of lava tubes in the light of observations at Mauna Ulu, Kilauea Volcano, Hawaii. Bull. Volcanol. (5), 343.
Richardson, P., Karlstrom, L., 2019. The multi-scale influence of topography on lava flow morphology. Bull. Volcanol. (4), 1.
Robl, J., Stüwe, K., Hergarten, S., 2008. Channel profiles around Himalayan river anticlines: constraints on their formation from digital elevation model analysis. Tectonics 27 (3).
Sapper, K., 1916. Die mittelamerikanische Landschaft. Geogr. Z. 8 (9), 489.
Sapper, K., 1925. Los volcanes de la America Central. Verland von Max Niemeyer, Halle.
Schenk, P.M., Williams, D.A., 2004. A potential thermal erosion lava channel on Io. Geophys. Res. Lett. 31 (23).
Siewert, J., Ferlito, C., 2008. Mechanical erosion by flowing lava. Contemp. Phys. (1), 43.
Sklar, L., Dietrich, W.E., 1998. River Longitudinal Profiles and Bedrock Incision Models: Stream Power and the Influence of Sediment Supply. Geophysical Monograph. American Geophysical Union, p. 237.
Staude, S., Barnes, S.J., Le Vaillant, M., 2017. Thermomechanical erosion of ore-hosting embayments beneath komatiite lava channels: textural evidence from Kambalda, Western Australia. Ore Geol. Rev. 90, 446–464.
Strozzi, T., Werner, C., Wiesmann, A., Wegmuller, U., 2012. Topography mapping with a portable real-aperture radar interferometer. IEEE Geosci. Remote Sens. Lett. (2), 277.
Tsang, S.W.R., Lindsay, J.M., Coco, G., Wysocki, R., Lerner, G.A., Rader, E., Turner, G.M., 2019. The heating of substrates beneath basaltic lava flows. Bull. Volcanol. (11), 1.
Turcotte, D.L., Turcotte, D.L., Schubert, G., 2002. Geodynamics. Cambridge University Press, Cambridge, New York.
Vincent, F., 1890. In and Out of Central America.
Voytenko, D., Dixon, T.H., Luther, M.E., Lembke, C., Howat, I.M., de la Peña, S., 2015. Observations of inertial currents in a lagoon in southeastern Iceland using terrestrial radar interferometry and automated iceberg tracking. Comput. Geosci. 82, 23–30.
Werner, C., Wegmüller, U., Strozzi, T., Wiesmann, A., 2000. Gamma SAR and interferometric processing software 1620, 1620.
Williams, D., Kadel, S., Greeley, R., Lesher, C., Clynne, M., 2004. Erosion by flowing lava: geochemical evidence in the Cave Basalt, Mount St. Helens, Washington. Bull. Volcanol. 2.
Williams, D.A., Kerr, R.C., Lesher, C.M., 1998. Emplacement and erosion by Archean komatiite lava flows at Kambalda: revisited. J. Geophys. Res. (B11), 27.
Williams-Jones, G., Williams-Jones, A.E., Stix, J., 1998. The nature and origin of Venusian canali. J. Geophys. Res., Planets 103 (E4), 8545.
Wilson, L., Head, J.W., 2017. Generation, ascent and eruption of magma on the Moon: new insights into source depths, magma supply, intrusions and effusive/explosive eruptions (Part 1: Theory). Icarus 283 (Lunar Reconnaissance Orbiter - Part II), 146–175.
Wooster, M.J., Wright, R., Blake, S., Rothery, D.A., 1997. Cooling mechanisms and an approximate thermal budget for the 1991-1993 Mount Etna lava flow. Geophys. Res. Lett. (24), 3277.
Xie, S., Dixon, T.H., Voytenko, D., Fanghui, D., Holland, D.M., 2018. Grounding line migration through the calving season at Jakobshavn Isbræ, Greenland, observed with terrestrial radar interferometry. Cryosphere 12 (4), 1387–1400.
Zum Gahr, K.-H., 1998. Wear by hard particles. Tribol. Int. (10), 587.